Off-specular x-ray scattering in Langmuir-Blodgett multilayers of a liquid-crystalline polymer

R. E. Geer,[1] S. B. Qadri,[2] and R. Shashidhar[1]
[1]*Code 6900, Naval Research Laboratory, Washington, D.C. 20375-5348*
[2]*Code 6600, Naval Resarch Laboratory, Washington, D.C. 20375-5348*

A. F. Thibodeaux and R. S. Duran
Department of Chemistry, University of Florida, Gainesville, Florida 32611
(Received 7 November 1994; revised manuscript received 21 February 1995)

The effect of surface roughness on the static layer undulations of multilayer films of a side-chain liquid-crystalline polymer has been investigated by off-specular x-ray scattering. The roughness correlation length evaluated from the off-specular data is shown to vary inversely with the average roughness of the multilayer film. The features of the off-specular x-ray scattering are similar to those exhibited by inorganic heterostructural films.

PACS number(s): 61.30.Eb, 68.18.+p, 36.20.Ey, 61.41.+e

INTRODUCTION

The anisotropic elastic nature of the smectic-A and smectic-C phases of liquid crystals has a tremendous impact on the penetration of roughness from a solid, bounding surface. Such smectic phases are characterized by quasi-long-range positional order (layering order) in one dimension and short-range positional order within the layer plane [1]. Due in part to the in-plane fluidity, the energy required for layer compression is large compared with that of layer bending. This leads to the propagation of the roughness from a boundary into the liquid crystal (in a homeotropic configuration) [2]. These surface-induced (static) undulations are different from the thermally excited undulations of the layers. Both x-ray and light scattering techniques have been used to study thermal layer undulations of smectic liquid crystals in bulk and in thin films [3,4]. Generally, for low molar mass thermotropic liquid crystals, the thermal fluctuations of the layers are very large and swamp the effects due to static undulations. Recently, it has been demonstrated that multilayer films of a side-chain, liquid-crystal polymer, formed by the Langmuir-Blodgett technique, possess a high degree of layer order due to a molecular level separation of the siloxane backbone and the mesogenic side groups [5]. This segregation drastically increases the layer compression modulus and hence diminishes the thermal layer fluctuations, permitting a quantitative study of the static undulations of the layers induced by the substrate surface.

We have recently carried out an investigation of the static undulations of a 30-layer liquid-crystal polymer film by examining the off-specular x-ray scattering [6]. By studying the diffuse scattering near several Bragg reflections and by using a theoretical model developed earlier [7], we were able to obtain quantitative values for the root-mean-square roughness (σ) of the layers, the in-plane correlation length (ξ) associated with the average layer undulation correlation function, and an exponent (h) related to the self-affine roughness of the layer interfaces. It was shown that the static layer undulations of the multilayer film are caused by the roughness associated with the monolayer of octadecyltrichlorosilane (OTS) chemisorbed onto the surface of the underlying silicon wafer. However, the dependence of (ξ) on the surface roughness has not been investigated.

In this paper we present the results of off-specular x-ray scattering studies on multilayer films of different thicknesses that have been deposited on substrates of varying roughness. The variations in multilayer root-mean-square roughnesses are shown to affect the in-plane roughness correlation function: the magnitude of the roughness correlation length increases with decreasing layer roughness. We also compare the features of the off-specular scans of the multilayers to those observed earlier for inorganic heterostructures [8].

EXPERIMENT

The liquid-crystal polymer used in the film deposition is a polysiloxane based copolymer of which 70% of the siloxane sites available for attachment are occupied by methyl groups. The liquid-crystalline mesogen, (R)-4'-(1-ethoxycabonyl-1-ethoxy)phenyl-4-[4-(9-decenoyloxy)-phenyl]benzoate, is attached to the remaining 30%. In the bulk, this material exhibits a stable smectic-C^* phase over a wide temperature range, extending to subambient temperatures [9]. Substrates used for deposition and x-ray diffraction were single crystal silicon wafers (100). These substrates were cleaned by soaking in Nochromix dissolved in concentrated sulfuric acid. Hydrophobization of the dry silicon wafers was achieved with a 2–5 vol % solution of octadecyltrichlorosilane (OTS) in 99% anhydrous hexadecane. Of the four hydrophobisized substrates investigated in this work, three were prepared simultaneously in the OTS-hexadecane solution in a humidity controlled dry box. The fourth was prepared in a glove bag in a stream of dry nitrogen. A computer controlled film balance (KSV LB5000) was used to prepare the multilayer Langmuir-Blodgett films [3]. Films were deposited using downstroke deposition (x deposition) in

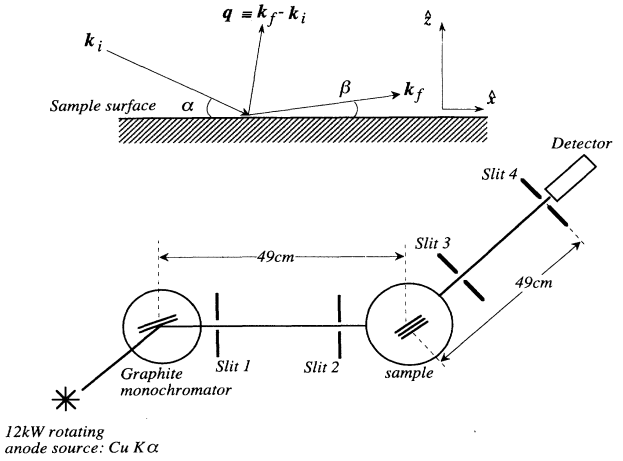

FIG. 1. Top: Scattering geometry for specular ($\alpha=\beta$) and off-specular ($\alpha\neq\beta$) scans. Bottom: Diffraction apparatus.

which the substrate was brought down through the monolayer into the subphase.

The x-ray beam (Rigaku RU-200 rotating anode source) used for diffraction was collimated by two tantalum slits place between the sample and the monochromator (graphite), and two more between the sample and the scintillation detector (Fig. 1). The in-plane resolutions are $\Delta q_x = 8\times10^{-4}$ Å^{-1} and $\Delta q_z = 1.1\times10^{-3}$ Å^{-1}. The out-of-plane resolution, $\Delta q_y \approx 0.2$ Å^{-1}, was determined primarily by the slit height. Measurements were performed at room temperature. The films were remarkably stable; x-ray diffraction patterns did not vary over periods exceeding six months.

The reciprocal space trajectories relevant to our investigations are shown in Fig. 2. The $\vec{z}$ axis is defined as the film normal. The $\vec{x}$ axis is perpendicular to this, in the scattering plane. The solid line at $q_x = 0$ traces the specular reflectivity trajectory (filled circles denote Bragg reflections). Rocking curves are shown as solid lines along q_x at approximately constant q_z and result from varying the sample orientation with respect to a fixed scattering angle. Due to refraction, the edges of these scans dip to lower values of q_z.

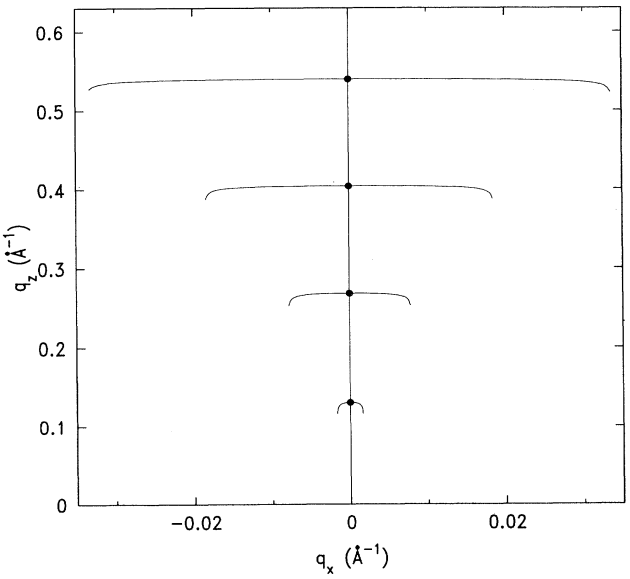

FIG. 2. Reciprocal space trajectories for x-ray scans. Specular scattering is measured along the solid line at $q_x = 0$. Rocking curves through Bragg reflections (filled circles) are approximately constant in q_z, except for the outermost edges which move to lower values of q_z due to refraction.

SPECULAR SCATTERING: MULTILAYERS

The specular and off-specular scattering of four multilayer samples consisting of 13, 50, 50, and 100 transferred monolayers was measured. As shown in Ref. [10], upon successive transfers the side-group mesogens of one copolymer layer reorient and interdigitate with respect to the side groups of the adjacent layer. Consequently, the multilayer develops a bulklike smectic structure in which the number of smectic layers is approximately 60% of the number of transferred monolayers. Figure 3 displays the intensity of specularly reflected x-rays for these multilayer samples (denoted $M1$–$M4$). These scans are along the ($00L$) axis of the multilayers, which coincides with the

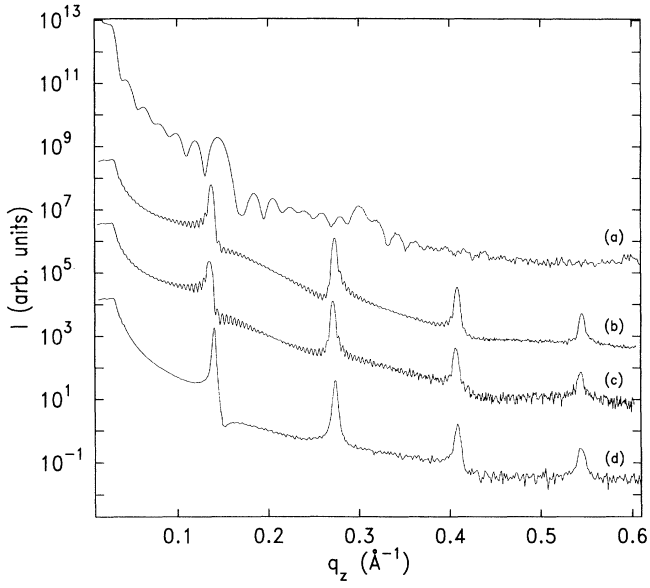

FIG. 3. Specular scattering from multilayers (a) $M1$, (b) $M2$, (c) $M3$, and (d) $M4$. The layer spacings (corrected for refraction) are 42.0, 47.4, 47.8, and 45.8 Å, respectively. The Bragg reflections present in the data reveal well-defined smectic layers in the film. The lack of third and fourth order reflections in the $M1$ reflectivity results from a larger rms layer roughness (see text) and the relatively few number of layers. The modulation in the amplitude of the subsidiary maxima (Kiessig fringes) seen in the $M1$, $M2$, and $M3$ film data is discussed in the text.

substrate normals. The Bragg reflections indicate well-ordered smectic layers with spacings $d=42.0$ Å ($M1$), $d=47.4$ Å ($M2$), $d=47.8$ Å ($M3$), and $d=45.8$ Å ($M4$). All values have been corrected for effects due to refraction. The appearance of subsidiary maxima (sometimes referred to as Kiessig fringes) between the Bragg reflections from the $M1$, $M2$, and $M3$ multilayers results primarily from interference between x rays reflected from the top and bottom surfaces of the film. Their spacing is inversely proportional to the film thickness. The observation of these fringes, into the third zone, implies a high degree of definition and relatively low mosaicity of the smectic layers. No Kiessig fringes could be resolved for the $M4$ multilayer due to the large thickness and spectrometer resolution.

When the film thickness is an integral multiple of the layer spacing, the number of fringes equals $N-2$, where N is the layer number. Figure 3 shows 6, 28, and 29 fringes in the specular scattering from the $M1$, $M2$, and $M3$ multilayers, respectively, implying $N_{M1}=8$, $N_{M2}=30$, and $N_{M3}=31$. The fringe widths yield thicknesses D of 320±10 Å ($M1$), 1451±6 Å ($M2$), and 1503±6 Å ($M3$). Using these thicknesses and the layer spacings calculated above, the number of smectic layers (N) for the films are $N_{M1}=7.6\pm0.24$, $N_{M2}=30.6\pm0.12$, and $N_{M3}=31.4\pm0.12$. Note that these calculated values for N are nonintegral. The thickness of the $M4$ multilayer can be approximated by extrapolating the ratio of transferred monolayers to smectic layers, determined from the Kiessig fringes of the first three samples. This yields a thickness of 62±2 smectic layers, or approximately 2840 Å. These ratios compare well with those calculated in Ref. [10].

It can be seen that the amplitude of the Kiessig fringes (observed between successive Bragg reflections) is modulated, possessing a minimum midway between Bragg peaks. Previous analysis from other multilayers has shown that this results from incoherent interference between x rays scattered from regions of the film that differ in thickness by one smectic layer [11,12]. This modulation is apparent for the $M1$, $M2$, and $M3$ specular data at $q_z=0.23$, 0.20, and 0.20 Å^{-1}, respectively. The extinction of the subsidiary maxima in the center of the second zone implies nearly equal contributions from both regions. Hence $M1$ consists of approximately $(7+8)/2$ layers, $M2$ of $(30+31)/2$ layers, and $M3$ of $(31+32)/2$ layers, reconciling the nonintegral values of N calculated from the fringe width. Recent atomic force microscopy measurements of these films reveal "patches" of a single smectic layer on the surface extending over the length scale of micrometers [13], consistent with what would be expected for an incoherent superposition of scattered x rays (the coherence length of the Cu Kα x rays <5000 Å).

SPECULAR SCATTERING: SUBSTRATES

To characterize their roughness and for comparison with the specular scattering from the multilayers, the specular reflectivity of the bare substrates was measured. All four substrates consisted of 100 silicon wafers. These were made hydrophobic through the chemisorption of an OTS monolayer. Those used for the $M2$, $M3$ and $M4$ multilayers were made hydrophobic in the same solution, separately from the $M1$ substrate (see experiment section). Specular reflectivity from the $M2$ substrate is shown in Fig. 4 (taken from Ref. [6]). The reflectivity is analyzed using a block density model consisting of four strata of distinct density ρ_i and thickness d_i whose interfaces are approximated by Gaussian smeared steps of width σ_i [14]:

$$\langle\rho(z)\rangle=\sum_{i=0}^{3}(\rho_i-\rho_{i+1})\mathrm{erf}\left[\frac{z-L_i}{\sqrt{2}\sigma_i}\right], \quad (1)$$

where $L_i=\sum_{j=0}^{i}d_j$. The measured intensity is given by

$$S(q_z)=R_F\left|\int_{-\infty}^{\infty}dz\frac{d\langle\rho(z)\rangle}{\rho_{-\infty}dz}e^{iq_zz}\right|^2, \quad (2)$$

where R_F is the Fresnel reflectivity for an ideal interface. The solid line in Fig. 4 results from a best fit to this model. The fitting parameters are shown in Table I and are in excellent agreement with previous reflectivity studies of similar monolayers [14]. The electron density profile is shown in the inset of Fig. 4. The value for the roughness of the chemisorbed monolayer-air interface is 3.3±0.3 Å. Specular scatterings from the $M3$ and $M4$ substrates are nearly identical with equal monolayer-air interfacial widths (to within uncertainty values). This is not surprising, since these were made hydrophobic simultaneously.

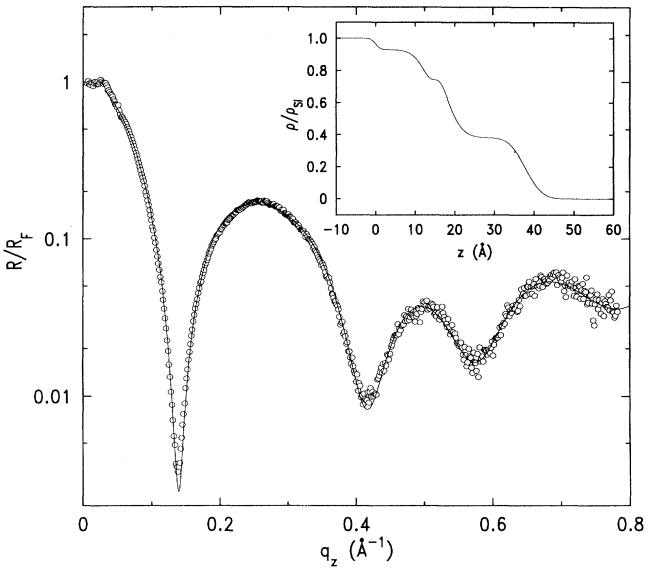

FIG. 4. Specular reflectivity from a bare portion of the hydrophobic substrate used in the deposition of the $M2$ multilayer. The solid line denotes the best fit to the model described in the text and in Ref. [6]. The corresponding electron density profile is shown in the inset. This is in very good agreement with reflectivity from chemisorbed monolayers of the same material from Ref. [14]. The fitting parameters are listed in Table I.

TABLE I. Fitting parameters for the octadecyltrichlorosiloxane monolayer reflectivities. The upper set of values corresponds to the data in Fig. 4 and was taken from Ref. [6]. The lower set of values corresponds to the data in Fig. 5. Parameters without uncertainty values were not varied during the fitting.

Layer	Silicon	Silicon oxide	SiO_2-silane interface	Alkyl chain
1 (Å)	∞	15.0±0.6	1.0	21.8±0.5
ρ/ρ_{Si}	1.0	0.93±0.02	1.22±0.04	0.38±0.03
σ (Å)	1.0	1.5±0.3	3.8±0.4	3.3±0.3
1 (Å)	∞	13.1±0.5	5.8±0.6	21.0±0.7
ρ/ρ_{Si}	1.0	0.93±0.03	0.43±0.03	0.36 ±0.04
σ (Å)	2.1±0.3	4.3±0.4	2.2±0.2	4.7±0.3

Specular reflectivity from the $M1$ substrate is shown in Fig. 5. The same analysis methodology was used. The fitting parameters for this film are shown in Table I. This fit is represented by a solid line in Fig. 5. The corresponding electron density profile is shown in the inset of Fig. 5. With the exception of the OTS–native-oxide interfacial region, the thickness and electron density of this film are similar to the other substrates. However, the $M1$ substrate is considerably rougher. The monolayer-air interfacial width is 4.7±0.3 Å compared to 3.3±0.3 Å for the $M2$ substrate. This difference most likely originates in the different deposition conditions of the monolayers. The thicker OTS–native-oxide interfacial region of the $M1$ substrate points to increased oligomer concentration during deposition due, possibly, to excess water [15]. This may also be responsible for the overall increased roughness.

The most obvious result of this greater roughness can be seen in Fig. 3. Note that for the $M1$ film the specular scattering is within the noise for $q_z \geq 0.4$ Å^{-1}, concealing higher order reflections that are evident for the other films.

OFF-SPECULAR SCATTERING

It is evident from the scattering in Fig. 3 that well-defined smectic layers are present in these multilayers. Imperfections in these layers will scatter x rays out of the specular direction. Such off-specular scattering is hence a probe of the layer disorder. Figure 6 displays rocking curves across the first and second Bragg reflections from the $M1$ multilayer, revealing significant diffuse scattering. Figure 7 shows similar scans for the first three Bragg

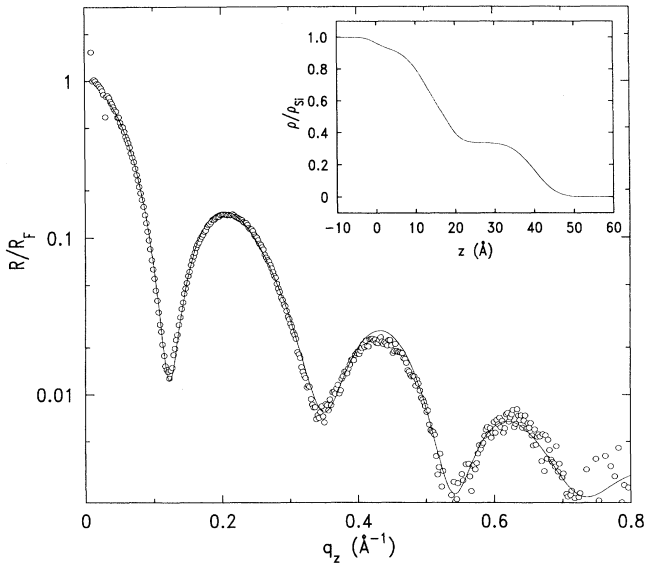

FIG. 5. Specular reflectivity from a bare portion of the hydrophobic substrate used in the deposition of the $M1$ multilayer. The solid line denotes the best fit to the model described in the text and in Ref. [6]. The corresponding electron density profile is shown in the inset. The profile is significantly rougher than that of Fig. 4. The fitting parameters are listed in Table I.

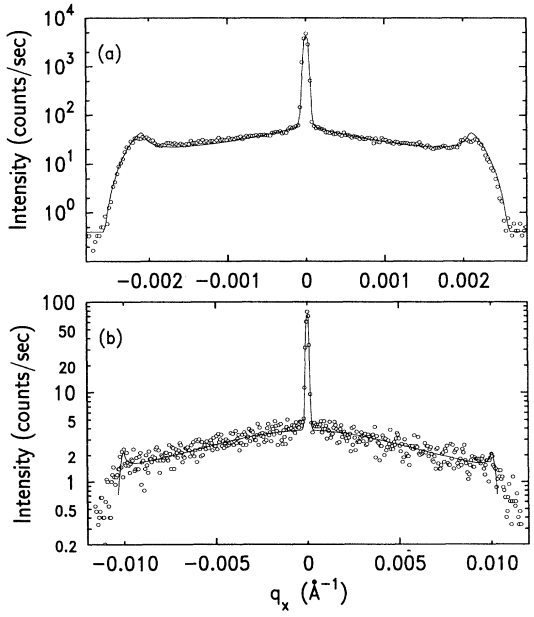

FIG. 6. Rocking curves through the first (top) and second (bottom) Bragg reflections of $M1$. The solid line is a fit to a model described in the text. Only three significant adjustable parameters were used in simultaneously fitting the data of both rocking curves. These are listed in Table II.

reflections from $M2$ (taken from Ref. [6]). The corresponding rocking curves from the $M3$ and $M4$ multilayers are presented in Figs. 8 and 9, respectively. Diffuse scattering as in Fig. 6 is present near each of the Bragg reflections from all of the multilayers. Note that there are subtle differences in the line shapes of the off-specular scattering for the various multilayers, even for multilayers of nearly the same thickness (Figs. 7 and 8). This indicates differences in the layer disorder or roughness between the films.

In smectic films such as we are considering, both of the primary sources of roughness, thermally excited layer undulations and penetration of substrate roughness, are governed by the smectic elastic constants, and in the case of thin films, also by the interfacial tensions. Consider substrate roughness penetrating smectic layers that are oriented parallel to the substrate surface. In the simplest model, the elastic free energy for the layer deformations of a uniaxial smectic is (neglecting anharmonic terms) [2]

$$F=\int d\vec{r}\left\{\frac{B}{2}\left[\frac{du}{dz}\right]^2+\frac{K}{2}[\Delta_\perp u(\vec{r})]^2\right\}, \tag{3}$$

where B and K are the layer compressive elastic constant and splay elastic constant, respectively, and $u(\vec{r})$ is the layer displacement field. Following de Gennes [2], consider a homeotropically oriented smectic sample. Enforce a sinusoidal displacement at the boundary that decays exponentially as one moves away from that boundary, i.e., $u(x,z)=\cos(q_x x)\exp(-z/L)$. Functional minimization of the free energy in Eq. 3 with respect to this boundary condition yields

$$L=\frac{1}{\sqrt{K/B}\,q_x^2}\ . \tag{4}$$

Thus, the penetration of an induced roughness is inversely proportional to the square of the undulation wave vector. The factor $(K/B)^{1/2}$ is usually denoted by λ and is a characteristic length scale for the bending of the layer. For small λ, the layer compressive elastic constant B is large compared to K. In this case it is energetically more costly to relax an undulation by local changes in the layer spacing, and therefore the undulation propagates, i.e., L is large. For large λ, local compression or expansion of the layer spacing is comparable in cost to the layer bend-

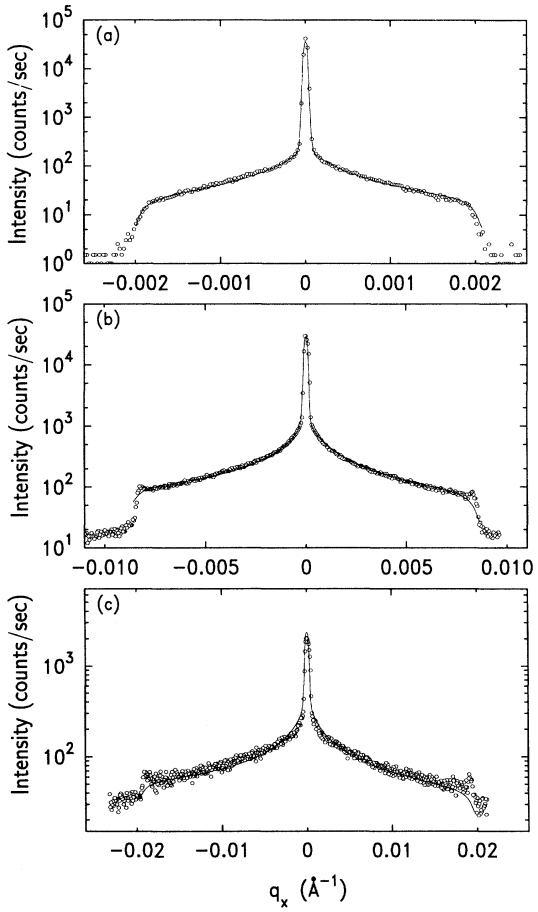

FIG. 7. Rocking curves through the first (top), second (center) and third (bottom) Bragg reflections of $M2$. These data are reprinted from Ref. [6] for direct comparison with Figs. 6, 8, and 9. The fitting parameters are listed in Table II.

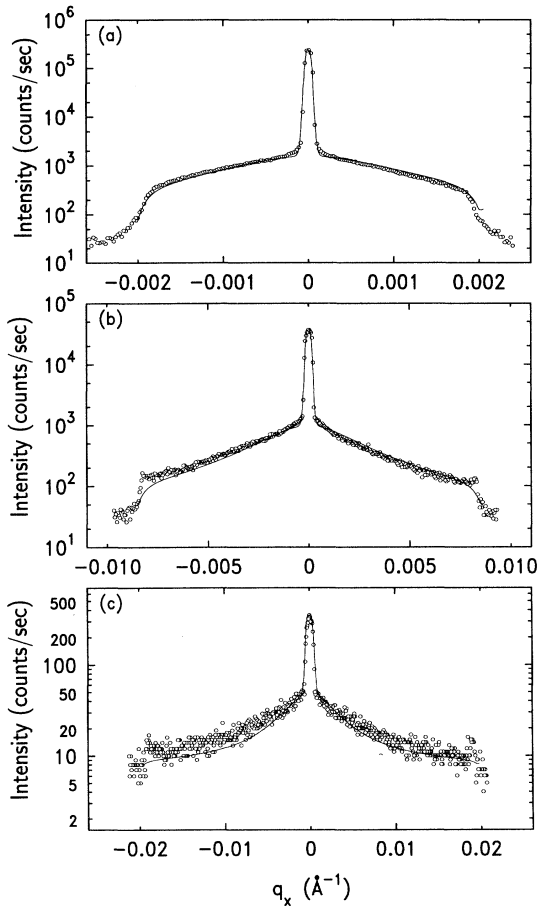

FIG. 8. Rocking curves through the first (top), second (center), and third (bottom) Bragg reflections of $M3$. The solid line is a fit to a model described in the text. The fitting parameters are listed in Table II.

ing energy, and undulations will damp out over distance and L will decrease.

For polysiloxane based liquid-crystalline polymers that are similar in structure to that studied here, Davidson and Levelut have estimated λ to be on the order of 2 Å [16]. Using the approximate values of q_x at the edges of the 001, 002, and 003 rocking curves in Figs. 7–9, $L_{\min}=1.54\times10^5$, 7800, and 1.540 Å, respectively, for each of these scans. For diffuse scattering near the first two Bragg reflections, substrate roughness penetrates the films virtually undamped. Only for the 003 rocking curve from the $M4$ multilayer is the film thickness larger than $L_{\min}$. This is discussed in more detail below.

For a quantitative model of the diffuse scattering in these multilayers, recall the general expression for the specular and off-specular scattering from a one-dimensionally modulated system. This has been given by Sinha *et al.* [7]:

$$I\cong\frac{I_0}{q_z^2\sin(\alpha)\sin(\beta)}\int\int dz'dz\frac{d\rho(z)}{dz}\frac{d\rho^*(z')}{dz'}\int\int dx\,dy(e^{q_z^2C(x,y,z-z')}e^{-i\vec{q}_\perp\cdot\vec{r}_\perp})e^{-iq_z(z-z')}. \tag{5}$$

I_0 is the incident intensity, α and β are the entrance and exit angles associated with incident and scattered x rays, $\rho(z)$ is the multilayer electron density profile and $C(x,y,z-z')$ is the interfacial height-height correlation function $\langle z(x,y)z(0)\rangle$. Assume that the scattering in Figs. 6–9 is dominated by roughness penetrating from the substrate. In that case C will resemble correlation functions from solid surfaces (at least over the length scales we are considering). For many isotropic solid surfaces the ensemble averaged roughness $g(R)=\langle[z(R)-z(0)]^2\rangle=AR^{2h}$, where $R=\sqrt{(x-x')^2+(y-y')^2}$. This describes the so-called self-affine roughness. For systems of finite size (and measurement techniques with limited spatial resolution) $g(R)\to2\sigma^2$ for large R, where σ is the rms roughness of the surface. A functional form satisfying these limits is [17]

$$g(R)=2\sigma^2[1-e^{-(R/\xi)^{2h}}]=2\sigma^2-2C(R). \tag{6}$$

Hence,

$$C(R)=\sigma^2\exp[-(R/\xi)^{2h}]. \tag{7}$$

ξ is an in-plane long distance cutoff. The simplest generalization of Eq. (7) to the case of multilayers is the addition of a factor $\exp[-(z-z')/\xi_\parallel]$, which accounts for decaying correlations along the layer normal [7]. For conformal roughness this term is close to unity. If this assumption is made and Eq. (7) is used for C, the integrations along and perpendicular to the layer normal in Eq. (5) can be separated. Expanding the exponential containing C yields the following expression:

$$I(q)=\frac{1}{q_z^2}F(q_z,\alpha,\beta)\left\{2\pi\delta(q_z)+\sum_{n=1}^{\infty}\frac{(\sigma^2q_z^2)^n}{n!}\int_{-\infty}^{\infty}dx\,e^{-n(|x|/\xi)^{2h}}e^{-iq_xx}\right\}. \tag{8}$$

The function $F(q_z,\alpha,\beta)$ represents the specularly reflected intensity. The first term in braces is the specular contribution at $q_x=0$, while the remainder of the summation represents the diffuse component. Seven terms of this series were retained to describe the diffuse scattering at the Bragg reflections. This function was convolved with the instrument resolution and incorporated into a nonlinear least-squares-fitting algorithm. Only three significant adjustable parameters, h, σ, and ξ, were varied for the fitting of each set of rocking curves for the $M1$, $M2$, $M3$, and $M4$ multilayers. The results are given in Table II. Those for the $M2$ multilayer are taken from Ref. [6]. The fits, in excellent agreement with the data, are shown as solid lines in Figs. 6–9.

As stated above, the penetration length for static undulations is dependent upon the scattering vector q_x. For the $M4$ multilayer the calculated value of the roughness penetration length is less than the film thickness for $|q_x|>0.013$ Å^{-1}. This encompasses 181 out of 563 data points in the 003 rocking curve and out of 1083 data points for the entire $M4$ data set, shown in Fig. 9. Inclusion of the data beyond $q_x=\pm0.0133$ Å^{-1} does not result in changes of the three fitting parameters outside the uncertainties shown in Table II. Similarly, if the 003 data are fitted separately, inclusion of these points does not change the values of the fitting parameters beyond the uncertainty values determined from $|q_x|<0.0133$ Å^{-1}. This is due in large part to the noise in the data beyond $q_x=\pm0.0133$ Å^{-1}. There is insufficient data to fit only those points for which L is larger than the film thickness and expect meaningful results. In light of this we do not take into account roughness that does not penetrate the multilayer in our analysis. To do this would require a much thicker film (which introduces practical difficulties in the Langmuir-Blodgett transfer) or several higher order Bragg reflections.

The roughnesses for the $M2$, $M3$, and $M4$ multilayers shown in Table II are all just slightly higher than the

TABLE II. Fitting parameters from Eq. (7) for the data in Figs. 6–9. The parameters for $M2$ are taken from Ref. [6]. There is no monotonic relationship between the film thickness and any of the parameters. The correlation length (ξ), however, is inversely related to the rms roughness (σ) of the multilayer.

Multilayer	Thickness (Å)	σ (Å)	ξ (Å)	h
$M1$	320±10	4.54±0.2	469±35	0.37±0.07
$M2$	1451±6	3.60±0.12	1327±18	0.25±0.05
$M3$	1503±6	4.00±0.15	911±22	0.5±0.05
$M4$	2840	3.83±0.12	922±20	0.10±0.03

monolayer-air interfacial widths determined from the substrate specular reflectivity (Table I), but agree well at the two standard deviation levels. The corresponding values for the $M1$ film agree very well. All these values confirm the earlier assumption that the layer disorder results primarily from surface-induced roughness. The flux associated with the rotating anode source provided an insufficient signal-to-noise ratio to permit a rocking curve analysis of the hydrophobic silicon substrate similar to that of the multilayers. It would be of great interest to perform such measurements at a synchrotron source for a direct comparison with the off-specular scattering from the multilayers.

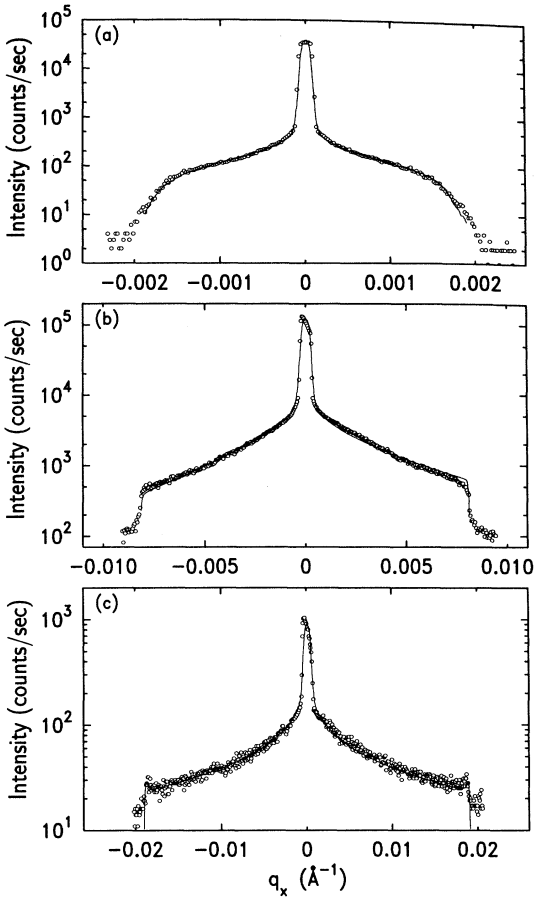

FIG. 9. Rocking curves through the first (top), second (center), and third (bottom) Bragg reflections of $M4$. The solid line is a fit to a model described in the text. The fitting parameters are listed in Table II. Note the difference in the line shapes of the diffuse scattering near $q_x=0$ compared to the data in Figs. 7 and 8. This results from changes in the roughness correlation function penetrating the smectic layers from the substrate.

Turning back to the results in Table II there is no monotonic relationship between any of the quantities and the film thickness. For layer undulations dominated by substrate roughness this is not unexpected if the film thickness is less than the layer undulation penetration length. Even for the $M2$ and $M3$ multilayers, which are of nearly the same thickness, the exponent h and the correlation length ξ are significantly different, further demonstrating that the off-specular diffuse scattering is not inherent to the liquid-crystal polymer, but rather depends on external factors, in this case the substrate surface. There is, however, a monotonic relationship between the rms roughness and the roughness correlation length in Table II. This translates into a much flatter line-shape in the off-specular diffuse scattering for increased interlayer roughness.

There is no such monotonic relationship between the exponent h and any other aspect of the films, except that the films with lower roughness tend to have lower values of h. In the conventional definition of self-affine roughness h is related to the surface or interfacial fractal dimension [18]: $D_S=3-h$. An interface with a Gaussian correlation function ($h=1$) possesses a fractal dimension of 2; for $h=0.5$ (exponential decay) $D_S=2.5$. However, Krim and Indeku [19] have recently pointed out that the correct interpretation of h depends on the relevant length scale. Specifically, for microscopic length scales small values of h imply increasing roughness, whereas in the thermodynamic limit ($R\rightarrow\infty$) decreasing values of h are indicative of smoother surfaces. Since an asymptotic limit is incorporated into the definition of $g(R)$ in Eq. (6), we subscribe to the former interpretation, which would imply more jagged interfaces for the $M2$ and $M4$ films. This has yet to be confirmed with a truly microscopic probe.

THERMAL UNDULATIONS

The above off-specular analysis is predicated on the dominance of substrate-induced static undulations. However, it has already been pointed out that the thermal undulations will also produce similar diffuse scattering. From the simple free energy in Eq. (1) the rms undulation

amplitude σ can be calculated for a smectic sample with a thickness D along the smectic normal and infinite dimensions parallel to the layers [20],

$$\sigma^2=\langle u^2(\vec{r})\rangle \approx \frac{k_B T}{4\pi\sqrt{KB}} \ln\frac{\sqrt{\lambda D}}{a_0} . \quad (9)$$

In the above expression a_0 is a short wavelength cutoff, approximately 5 Å for the polymer side chains. Measured values of K in side-chain polymers are very close to monomer values, on the order of 1×10^{-6} dyn [21]. Using the estimation of λ from Ref. [16], $B\approx2.5\times10^9$ dyn/cm^2, which yields $\sigma=1.3$ Å for $D=1500$ Å. The corresponding value for a monomer ($B\approx2.5\times10^7$ dyn/cm^2 [20]) film is 5.0 Å. This amplitude increases logarithmically with D due to the one-dimensional nature of the smectic mass density wave.

From this simple estimation we conclude that thermal undulations cannot account for the observed layer roughness extracted from the data in Figs. 6–9. We can extend this calculation to determine the thermal undulation correlation function for direct comparison with Eq. (7). Following Holyst [20], we define an elastic free energy for a finite size smectic film,

$$F=\int d\vec{r}\left\{\frac{B}{2}\left[\frac{du}{dz}\right]^2+\frac{K}{2}[\Delta_\perp u(\vec{r})]^2\right\} + \int d\vec{r}_\perp\{\gamma_2|\nabla_\perp u(\vec{r})|^2_{z=Nd}\} + \int d\vec{r}_\perp\{\gamma_1|\nabla_\perp u(\vec{r})|^2_{z=0}\} . \quad (10)$$

γ_1 is the film-vapor surface tension. At the interface with the silicon substrate we define the boundary condition $u(\vec{r})=0$ [22]. Both of these additions will tend to decrease the value of σ calculated above. The undulation correlation function for a finite number of smectic layers is most easily calculated by discretizing $u(\vec{r})$ along the $\vec{z}$ axis:

$$F=\tfrac{1}{2}\int dr_\perp\left[\sum_{n=0}^{N'-1}\frac{B}{d}[u_{n+1}(r_\perp)-u_n(r_\perp)]^2 + \sum_{n=0}^{N'} Kd[\Delta_\perp u_n(r_\perp)]^2 + \gamma_1|\nabla_\perp u_0(r_\perp)|^2\right] . \quad (11)$$

d is the layer spacing and $N'=N-1$. Upon Fourier transformation the free energy is quite simply expressed as

$$F=\tfrac{1}{2}\int d\vec{q}_\perp \sum_{k,n=0}^{N} u_k(\vec{q}_\perp)M_{kn}u_n(-\vec{q}_\perp) . \quad (12)$$

M_{kn} is a tridiagonal matrix (see Ref. [20] for the definitions of the elements). Invoking the equipartition theorem [23],

$$\langle u_n(r_\perp)u_n(0)\rangle=\frac{k_B T}{(2\pi)^2}\int d\vec{q}_\perp(M^{-1})_{nn}e^{i\vec{q}_\perp\cdot\vec{r}_\perp} . \quad (13)$$

Using the previous estimations for B and K, $d=47.4$ Å and $\gamma=30$ dyn/cm, this expression was used to calculate the undulation correlation function at the centers of 8-, 30-, and 62-layer films. These are plotted (along with the measured correlation functions of the four multilayers) in Fig. 10. It is clear the thermal undulations are a minor contribution, supporting our previous assumption that roughness in these polymer films results primarily from the substrate. It is interesting to note that for small values of λ, such as in the polymer case, the correlation function calculated from Eq. (13) changes very little over the profile of the film, i.e., thermal fluctuations for highly incompressible, thin smectic films are nearly conformal.

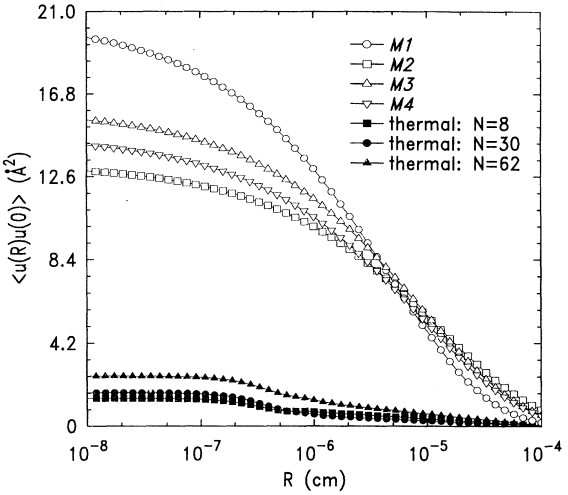

FIG. 10. Measured roughness correlation functions $C(R)$ for the $M1$ (open circles), $M2$ (open squares), $M3$ (open triangles), and $M4$ (open inverted triangles) multilayers. For comparison, the calculated thermal undulation correlation function for the center of 8-layer (solid squares), 30-layer (solid circles), and 62-layer (solid triangles) polymer films are also plotted. The thermal undulations represent a minor contribution to the overall roughness. Solid lines are a guide to the eye.

COMPARISON WITH INORGANIC MULTILAYERS

Similar diffuse scattering has been seen in inorganic multilayers especially those studied for applications in x-ray optics in which a uniaxial density modulation is desired with no in-plane order. Such a structure is not unlike the smectic films studied here. To facilitate such a comparison Figs. 11 and 12 give a more complete view of reciprocal space by plotting rocking curves from the $M2$ multilayer at various positions along the q_z axis. Successive scans have been offset for clarity. The intensity at the outermost edges of each rocking curve sets the level of background scattering for the scan. It is clear that the off-specular scattering in Figs. 6–9 is peaked at the Bragg reflections constituting diffuse "streaks" across the specular ridge of scattering. The lack of modulation at finite q_x implies no in-plane modulation. This is extremely similar to the diffuse scattering reported by Savage *et al.* [24] and Kortright in inorganic multilayer heterostructures [8].

For many of the rocking curves, especially for $q_z < q_B = 0.135$ Å^{-1} (the Bragg position), small peaks are evident at the edges of the scan. The origin of these so-called Yoneda wings [25] is an enhanced scattering amplitude resulting from standing waves that form at the surface of the film due to the interference of incident and totally externally reflected x rays when either α or β is near the critical angle. These should not be confused with the peaks seen in the rocking curves at $q_z = 0.144$, 0.163, 0.278, and 0.283 Å^{-1}. The latter result from the trajectory of the rocking curves, shown in Fig. 2. Rocking curves centered just above Bragg reflections will cross into the diffuse streaks of scattering when either α or β approaches the critical angle [8]. Also evident in the rocking curves near the first Bragg reflection are small satellite peaks that occur at negative (positive) values of q_x for $q_z < (>) q_B$ (Fig. 13). In fact these peaks occur precisely where $\beta = \theta_B$ (the Bragg angle). Kortright discusses standing wave enhanced diffuse scattering in the case of inorganic multilayers wherein x rays incident at the Bragg condition set up standing waves that enhance diffuse scattering [26], but this occurs only for the *entrance angle* $\alpha = \theta_B$, not the exit angle. No evidence of such scattering at $\alpha = \theta_B$ is seen here. It is most likely that the satellite peaks in Fig. 13 originate in a dynamical process, i.e., multiple scattering in which photons scattered at θ_B are coupled via a nonzero q_x component to the nearby first order Bragg reflection [8].

In the cases for both organic and inorganic multilayers

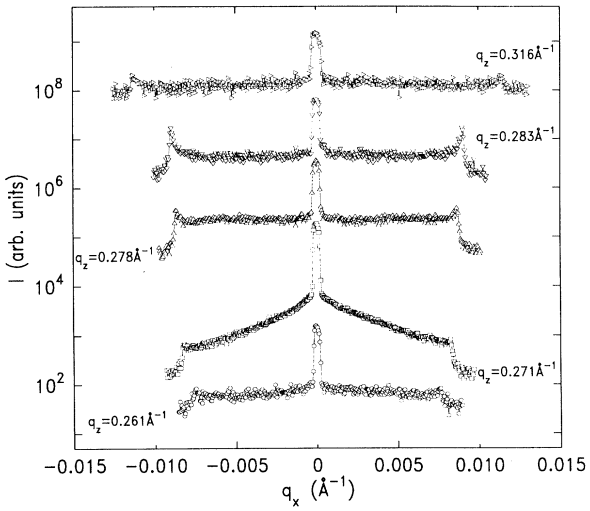

FIG. 12. Rocking curves near the second multilayer Bragg reflection of $M3$. Scans are offset for clarity. The diffuse scattering at the second order Bragg reflection is clearly evident. Solid lines are a guide to the eye.

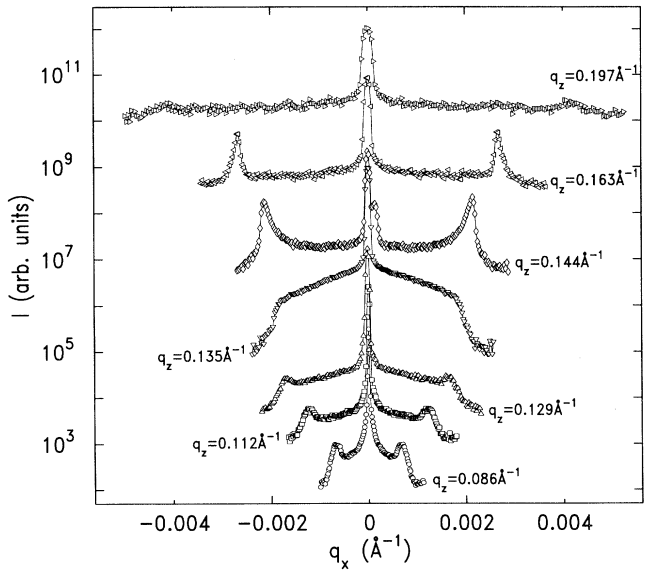

FIG. 11. Rocking curves in the vicinity of the first Bragg reflection from the $M3$ multilayer. Scans are offset for clarity. A large diffuse scattering is seen near the Bragg reflection. The lack of modulation in q_x implies that this scattering is not associated with an in-plane modulation. The peaks at the outer edges of the rocking curves at $q_z = 0.086$, 0.112, 0.129, and 0.197 Å^{-1} are the so-called Yoneda wings, discussed in the text. Similar peaks evident at $q_z = 0.144$ and 0.163 Å^{-1} are due to the rocking curve trajectory and originate from the diffuse scattering at the nearby Bragg reflection. Solid lines are a guide to the eye.

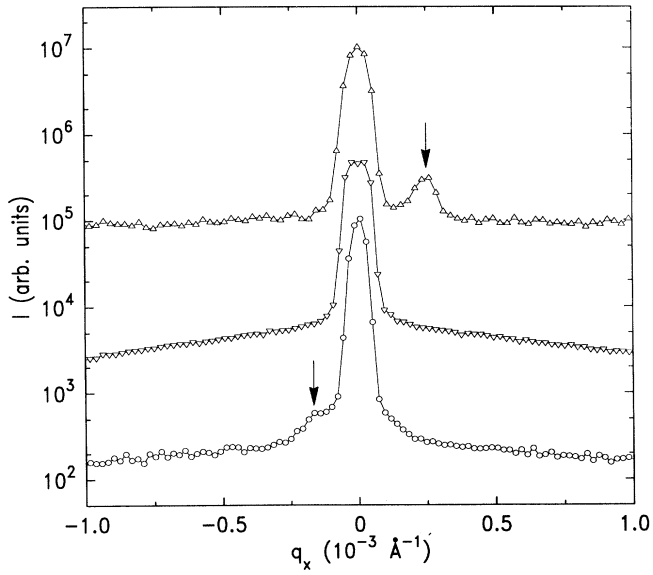

FIG. 13. Detail of rocking curves at and near the first Bragg reflection of $M3$. $q_z = 0.149$ Å^{-1} (triangles), 0.135 Å^{-1} (inverted triangles) and 0.125 Å^{-1} (circles). Scans are offset for clarity. The arrows point out small satellite peaks which occur when the *exit angle* of scattered x rays equals the Bragg angle. These features are discussed in the text. Solid lines are a guide to the eye.

diffuse scattering is associated with layer disorder or roughness. Although the microscopic origins of such disorder between the two systems are markedly different, the layer roughness for either can be expressed as a combination of two limiting cases: layer interfaces that are totally uncorrelated or totally correlated. The latter case in both results in replication of substrate roughness throughout the multilayer stack. In the case of inorganic heterostructures uncorrelated layer roughness arises primarily from deposition kinetics (i.e., roughening) [24], while for the films studied here thermally excited layer undulations are primarily responsible for uncorrelated roughness. There is conflicting evidence, however, whether the diffuse streaks seen here and in Ref. [8] and in Ref. [24] imply correlation of the layer roughnesses. References [24] and [27] maintain that totally uncorrelated roughness will yield off-specular scattering with no modulation along q_z. This has been supported by direct calculation of diffuse scattering amplitudes from multilayers by Payne and Clemens [28] and Holy and Baumbach [29]. However, it was argued by Kortright [8] and shown theoretically by Stearns [30] and Holy *et al.* [31] that even for uncorrelated interfaces the constructive interference at a Bragg reflection will also enhance the scattering amplitude of x rays scattered in the off-specular direction. Hence, at this point it is not clear whether peaks in the off-specular scattering at Bragg reflections are sufficient evidence for correlation of multilayer interfaces.

CONCLUSION

In summary, we have measured the off-specular x-ray scattering from Langmuir-Blodgett films of liquid-crystalline copolymers. Diffuse peaks are observed that are indicative of layer disorder, namely, layer undulations. Quantitative analysis of this diffuse scattering reveals that these undulations are primarily static in nature, resulting from the penetration of roughness from the substrate. Due to the large elastic constants associated with the smectic layers of these polymers, thermal undulations represent a minor contribution to this disorder.

ACKNOWLEDGMENTS

It is a pleasure to acknowledge discussions with Dr. B. Ratna, Dr. L. Sorensen, and Dr. P. Davidson. The authors also thank Dr. J. Naciri for the sample. Part of this work was supported by a grant from the Office of Naval Research. One of us (R.E.G.) gratefully acknowledges financial support from the National Research Council.

[1] See, e.g., P. S. Pershan, *Structure of Liquid-Crystal Phases* (World Scientific, Singapore, 1988).
[2] P. G. de Gennes, *The Physics of Liquid Crystals* (Oxford University Press, London, 1974).
[3] R. Ribotta, D. Salin, and G. Durand, Phys. Rev. Lett. **32**, 6 (1974).
[4] D. J. Tweet, R. Holyst, B. D. Swanson, H. Stragier, and L. B. Sorensen, Phys. Rev. Lett. **65**, 2157 (1990); S. Gierlotka, P. Lambooy, and W. H. de Jeu, Europhys. Lett. **12**, 341 (1990).
[5] A. F. Thibodeaux, R. E. Geer, S. Qadri, J. Naciri, R. Shasihidhar, and R. S. Duran, Polym. Prept. Am. Chem. Soc. Div. Polym. Chem. **33**, 1220 (1992).
[6] R. E. Geer, R. Shashidhar, A. F. Thibodeaux, and R. S. Duran, Phys. Rev. Lett. **71**, 1391 (1993).
[7] S. K. Sinha, M. K. Sanyal, A. Gibaud, S. K. Satija, C. F. Majkrzak, and H. Homma, *Science and Technology of Nanostructured Magnetic Materials,* edited by G. C. Hadjipanayis and G. A. Prinz (Plenum, New York, 1991).
[8] J. B. Kortright, J. Appl. Phys. **70**, 3620 (1991).
[9] J. Naciri, S. Pfeiffer, and R. Shashidhar, Liq. Cryst. **10**, 585 (1991).
[10] R. E. Geer, S. B. Qadri, R. Shashidhar, A. F. Thibodeaux, and R. S. Duran, Liq. Cryst. **16**, 869 (1994).
[11] R. E. Geer, S. B. Qadri, and R. Shashidhar, Ferroelectrics **149**, 147 (1993).
[12] P. Lambooy, Ph.D. thesis, College van Hoogleraren, 1992 (unpublished).
[13] B. Peek (unpublished).
[14] I. M. Tidswell, B. M. Ocko, P. S. Pershan, S. R. Wasserman, G. M. Whitesides, and J. D. Axe, Phys. Rev. B **41**, 111 (1990).
[15] Abraham Ulman, *An Introduction to Ultrathin Organic Films* (Academic, New York, 1991).
[16] P. Davidson and A. M. Levelut, Liq. Cryst. **11**, 469 (1992).
[17] S. K. Sinha, E. B. Sirota, S. Garoff, and H. B. Stanley, Phys. Rev. B **38**, 2297 (1988).
[18] B. B. Mandelbrot, *The Fractal Geometry of Nature* (Freeman, New York, 1982).
[19] J. Krim and J. O. Indeku, Phys. Rev. E **48**, 1576 (1993).
[20] R. Holyst, Phys. Rev. A **44**, 3692 (1991).
[21] P. Fabre, C. Casagrande, M. Veyssie, and H. Finkelmann, Phys. Rev. Lett. **53**, 993 (1984).
[22] I. Entin, R. goffer, D. Davidov, and I. Hersht, Phys. Rev. B **47**, 8265 (1993).
[23] D. Forster, *Hydrodynamic Fluctuations, Broken Symmetry and Correlation Functions* (Addison-Wesley, Redwood City, CA, 1975).
[24] D. E. Savage, J. Kleiner, N. Schimke, Y. H. Phang, T. Janowski, J. Jacobs, R. Kariotis, and M. G. Lagally, J. Appl. Phys. **74**, 6158 (1993).
[25] Y. Yoneda, Phys. Rev. **131**, 2010 (1963).
[26] J. B. Kortright and A. Fischer-Colbrie, J. Appl. Phys. **61**, 1130 (1987).
[27] H. Zabel, Appl. Phys. A **58**, 159 (1994).
[28] A. P. Payne, and B. M. Clemens, Phys. Rev. B **47**, 2289 (1993).
[29] V. Holy and T. Baumbach, Phys. Rev. B **49**, 10 668 (1994).
[30] D. G. Stearns, J. Appl. Phys. **71**, 4286 (1992).
[31] V. Holy, J. Kubena, I. Ohlidal, K. Lischka, and W. Plotz, Phys. Rev. B **47**, 15 896 (1993).